Submillimeterwave Spectroscopy of and Interstellar Search for Nitrosomethane: CH3NO

Laurent Margules, Zachary T. P. Fried, Alex N. Byrne, Brett A. Mcguire, Luyao Zou, Roman A. Motiyenko, J.-C. Guillemin

The Astrophysical Journal, 986:136 (10pp), 2025 June 20 https://doi.org/10.3847/1538-4357/add47f

Submillimeterwave Spectroscopy of and Interstellar Search for Nitrosomethane: CH_3NO

Laurent Margulès[1], Zachary T. P. Fried[2], Alex N. Byrne[2], Brett A. McGuire[2,3], Luyao Zou[1,5], Roman A. Motiyenko[1], and J.-C. Guillemin[4]
[1] Univ. Lille, CNRS, UMR 8523—PhLAM, Physique des Lasers Atomes et Molécules, F-59000 Lille, France; laurent.margules@univ-lille.fr
[2] Department of Chemistry, Massachusetts Institute of Technology, Cambridge, MA 02139, USA
[3] National Radio Astronomy Observatory, Charlottesville, VA 22903, USA
[4] Univ Rennes, Ecole Nationale Supérieure de Chimie de Rennes CNRS, ISCR UMR6226, F-35000 Rennes, France
Received 2025 January 21; revised 2025 April 22; accepted 2025 April 26; published 2025 June 12

Abstract

New measurements of nitrosomethane (CH_3NO), a formamide isomer, were done up to 660 GHz. The molecule exhibits internal rotation motion from the CH_3 group, and therefore the analysis with a dedicated rho-axis method code, RAM36, was used. A total of 2035 lines for $v_t = 0$ and 1 states of A and E symmetries were fitted with an rms deviation of 41.1 kHz, with the maximum quantum numbers values $J = 30$ and $K_a = 15$. Using these new data, CH_3NO was searched in the cold dark cloud Taurus Molecular Cloud 1 as well as the high mass star-forming regions Sgr B2(N) and NGC 6334I. CH_3NO was not observed in any of the sources, 3σ column density upper limits were determined, and we discuss the implications for the chemistry of CH_3NO in the interstellar medium. The accurate spectroscopic prediction of its spectra provided in this work will allow astronomers to continue the search of CH_3NO in other interstellar sources.

Unified Astronomy Thesaurus concepts: Astrochemistry (75)

Materials only available in the online version of record: machine-readable table

1. Introduction

Among the more than 320 compounds detected in the interstellar medium (ISM) and circumstellar medium (B. A. McGuire 2022),[6] 6 contain a bond between nitrogen and oxygen: nitrosyl hydride (HNO; B. Ulich et al. 1977), nitrogen oxide (NO; H. Liszt & B. Turner 1978), dinitrogen oxide (N_2O; L. Ziurys et al. 1994), fulminic acid HCNO (N. Marcelino et al. 2008), trans-nitrous acid (HONO; A. Coutens et al. 2019), and hydroxylamine (H_2NOH; V. M. Rivilla et al. 2020). Except fulminic acid, all are inorganic compounds. Because most of the species detected in these media are organic compounds, (B. A. McGuire 2022), it was interesting to examine organic compounds with such an N–O bond and a small number of atoms. The two (saturated) methyl derivatives CH_3NHOH (L. Kolesniková et al. 2017) and CH_3ONH_2 (L. Kolesniková et al. 2018) are still not detected in the ISM, so we selected, after trans-formaldoxime (CH_2=NOH; L. Zou et al. 2021), the simplest alkyl derivative bearing a NO group, the nitrosomethane (CH_3NO) as the target compound. It could form in the ISM by the reaction of CH_3 with NO (D. Miller & E. Steacie 1951; M. I. Christie 1959a, 1959b; T. Wolff & H. G. Wagner 1988; J.-X. Zhang et al. 2005) or by oxidation of the methylamine (CH_3NH_2). About 30% of compounds observed in the ISM with more than two atoms have one or more known detected isomers. CH_3NO is an isomer of formamide (H_2NCHO), which is detected in abundance in the ISM (R. Rubin et al. 1971) and which is by 62.8 kcal mol^{-1} thermodynamically more stable (M. Lattelais et al. 2010). It is also an isomer of formaldoxime (CH_2=NOH), which is 11.8 kcal mol^{-1} more stable and whose millimetric spectrum has been recorded recently (L. Zou et al. 2021). Formally, CH_3NO and CH_2NOH are in tautomeric equilibrium ($RCH_2NO \rightleftharpoons RCH{=}NOH$), but in lab nitroso compounds are only stable when there is no hydrogen on the carbon connected to the nitrogen atom (J. A. Long et al. 2001; A. E. DePrince & D. A. Mazziotti 2010). CH_3NO is therefore a kinetically very unstable compound. In chemistry, the most important spin-trapping compounds are nitroso compounds, which react with radicals to give nitroxide radicals:

$$RNO + R'^{\bullet} \longrightarrow RR'NO^{\bullet}, \quad (1)$$

EEWa role that CH_3NO could play in the ISM if it is present in this medium. Several spectroscopic studies led to the recording of its electronic absorption (V. Bhujle et al. 1976), photoelectronic (D. Frost et al. 1982), and microwave spectra (D. Coffey et al. 1968; P. H. Turner & A. P. Cox 1978). P. H. Turner & A. P. Cox (1978) reported the microwave spectra of 10 isotopic species of CH_3NO and determined the dipole moment components: $\mu_a = 2.537$ D, $\mu_b = 1.062$ D, and $\mu = 2.750 \pm 0.006$ D.

We here report the reinvestigation of the rotational spectra of CH_3NO in the milli- and submillimeter-wave domains. We also present its search in the cold dark cloud Taurus Molecular Cloud 1 (TMC-1) as well as the high-mass star-forming regions Sgr B2(N) and NGC 6334I. Section 2 describes the synthesis method and the spectrometers used to record the spectra. Section 3 details the model and the strategy used to assign the spectra. Section 4 presents the results from the astronomical observations. Section 6 discusses the possible

[5] Current address: Université Littoral Côte d'Opale, Laboratoire de Physico-Chimie de l'Atmosphère UR 4493, 59140 Dunkerque, France.
[6] See also http://cdms.astro.uni-koeln.de/classic/molecules and http://www.astrochymist.org/astrochymist_ism.html.

formation process of CH_3NO, and finally Section 6 summarizes our conclusions.

2. Experimental Section

2.1. Synthesis

Commercially available t-butyl nitrite was purchased from Aldrich and used without further purification. To prepare CH_3NO, the Gowenlock and Lüttke synthesis (B. Gowenlock & W. Lüttke 1958) was modified by replacing photolysis with flash vacuum thermolysis (FVT). The vacuum line (10 Pa) was equipped with an oven heated to 500 °C connected to a U-trap immersed in a cold bath at −100 °C. FVT of t-butyl nitrite gave a mixture of acetone and CH_3NO. The acetone was selectively trapped in the U-tube, while the gaseous stream containing mainly more volatile CH_3NO was introduced into the spectrometer cell. When cooled in a U-tube immersed in a bath of liquid nitrogen, CH_3NO exhibits a deep blue color that turns yellow–brown after a few seconds when the cold bath is removed. Revaporization of small amounts of CH_3NO is possible, but direct analysis of the gas stream provides a simpler experimental procedure and gives a preparative approach.

2.2. Lille: Submillimeter-wave Spectra

The measurements in the frequency range under investigation (150–660 GHz) were performed using the Fast Lille Absorption emiSsion High resolution (FLASH) spectrometer (O. Zakharenko et al. 2015; R. A. Motiyenko et al. 2019; L. Zou et al. 2020), offering both high precision with frequency measurements and fast scanning spectral acquisition. It implements frequency multiplication chains based on Schottky diodes, covering the 50–1520 GHz range. Its special feature is the application of a direct digital synthesizer at the first stage of frequency multiplication, which provides frequency switching as fast as 6.4 ns/point and continuous phase stability. The FLASH spectrometer is particularly notable for incorporating the chirped-pulse technique. While this technique is well established in the centimeter range, its application in the THz domain is still innovative, making the FLASH spectrometer a unique and versatile tool capable of operating up to 1.5 THz in absorption mode and 0.5 THz in chirped-pulse mode.

The absorption cell was a pyrex tube (10 cm in diameter, 220 cm in length). Since CH_3NO was found to be unstable at room temperature even at low pressure, the pyrolysis had to be done in situ during measurements, then introduced into the Pyrex cell of the spectrometer in slow flow mode. A U-tube in a cold bath, using liquid nitrogen and pentane at −125 °C, was placed just before the pyrex cell in order to trap acetone. The measurements were made at room temperature, and the sample pressure was about 3.5 Pa. During our first measurement campaign, we employed chirped-pulse emission spectroscopy in the 150–500 GHz range. This technique offers the advantages of higher sensitivity and faster acquisition when using room-temperature Schottky detectors. However, compared to absorption spectroscopy, its inherent drawback is lower spectral resolution, resulting in frequency measurement uncertainties of at least 150 kHz.

In a subsequent campaign, we conducted measurements using conventional absorption spectroscopy with frequency modulation and second-harmonic (2f) lock-in detection in the 150–330 and 400–660 GHz ranges. Signals were detected using a liquid-helium-cooled InSb bolometer (QMC Instruments Ltd.). The linewidth was primarily limited by Doppler broadening, and the estimated frequency measurement uncertainty was 50 kHz—slightly higher than our usual 30 kHz uncertainty. This increase is attributed to a 25% larger frequency step, which enabled faster scans without significantly compromising sensitivity. Line frequencies were determined by least-squares fitting, either by modeling the line peak with a parabolic function or the full profile with a Voigt function. A larger frequency step reduces the number of fitted points, which in turn may affect the accuracy of frequency determination.

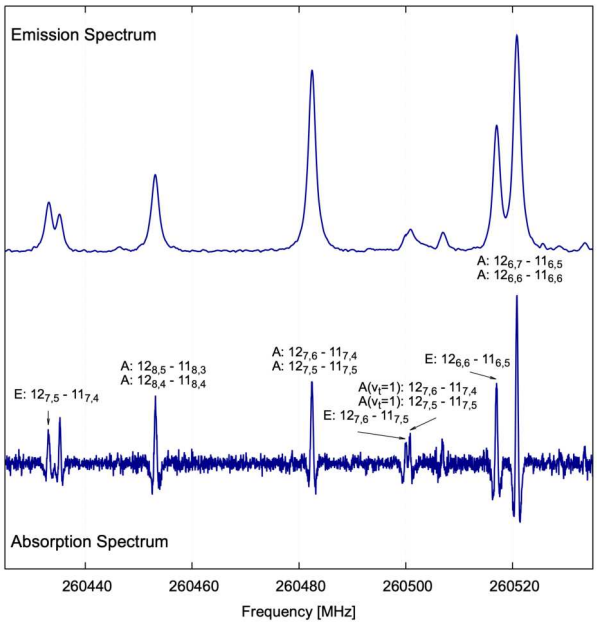

Figure 1. Part of nitrosomethane spectra recorded at 260.5 GHz using chirped-pulse emission spectroscopy (top) and conventional absorption spectroscopy with frequency modulation (bottom).

Figure 1 compares nitrosomethane spectra recorded using chirped-pulse emission spectroscopy (top) and conventional absorption spectroscopy with frequency modulation (bottom). Notably, absorption spectroscopy provides a three- to fourfold improvement in frequency resolution at the expense of a significantly lower signal-to-noise ratio. Ultimately, the emission spectroscopy measurements in the first campaign allowed us to optimize experimental conditions, while the absorption spectroscopy measurements in the second campaign were used for spectral analysis.

Figure 2 displays a segment of the broadband spectrum recorded using the FLASH spectrometer, alongside a stick spectrum representing a mixture of nitrosomethane and acetone. While the experimental and theoretical spectra exhibit overall similarity, noticeable discrepancies in intensity are observed across the shown range. These deviations can be primarily attributed to the kinetic instability of nitrosomethane and acetone formation during flash thermolysis. The stick spectrum was generated under the assumption of a 1:3 concentration ratio of nitrosomethane to acetone. This ratio accurately reproduces the intensities in the lower-frequency region; however, at higher frequencies, an increase in acetone concentration is evident. Additionally, inconsistencies in

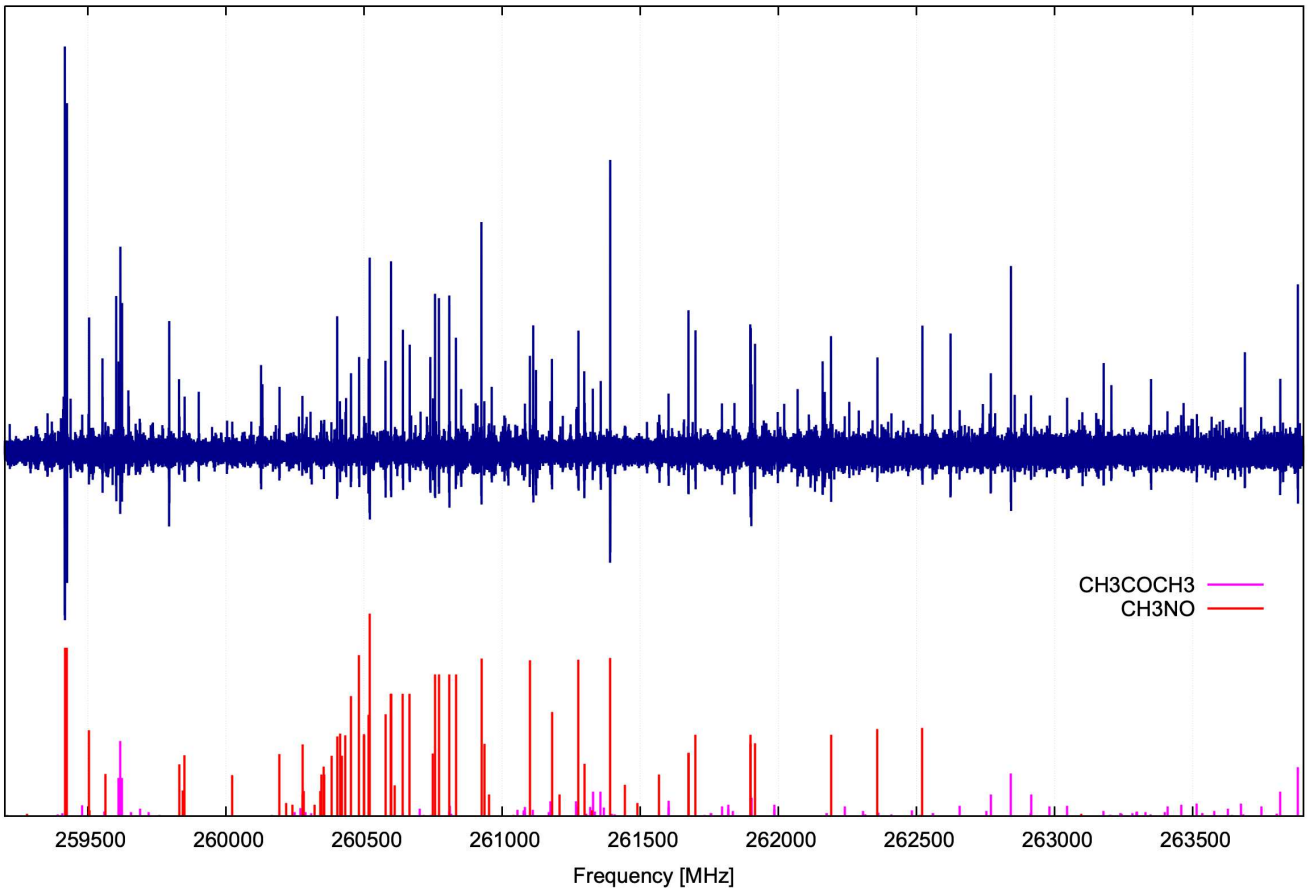

Figure 2. Experimental absorption spectrum (in blue) and modeled stick spectrum of CH_3NO and acetone $(CH_3)_2CO$. The intensities is the stick spectrum are scaled using the 1:3 ratio of CH_3NO:$(CH_3)_2CO$.

nitrosomethane intensities within a relatively narrow frequency range further highlight the rapid kinetic variations occurring in FVT.

3. Analysis of the Rotational Spectra

CH_3NO is an asymmetric near-prolate rotor ($\kappa \approx -0.95$). It has nonzero dipole components along the a- ($\mu_a = 2.537$ D) and b-axis ($\mu_b = 1.062$ D), as determined by P. H. Turner & A. P. Cox (1978). The molecule is challenging from a spectroscopic point of view as it exhibits large-amplitude methyl torsional motion, where the interaction between internal rotation of the methyl group and overall rotation of the molecule complicate spectral analysis. While CH_3NO possesses a medium-sized barrier to internal rotation ($V_3 \approx 416.4\,\mathrm{cm}^{-1}$), its nearly symmetric internal rotor geometry nevertheless leads to large $A - E$ splittings (D. Coffey et al. 1968; P. H. Turner & A. P. Cox 1978) up to several hundreds of MHz, and where A and E are the symmetry species of the C_{3v} symmetry point group characterizing the internal rotor. Another difficulty is the relatively high ratio of the methyl top moment of inertia to that of the rest of the molecule leading to a relatively large coefficient for the coupling term between internal rotation and global rotation ($\rho = 0.35$). The case is very similar to ^{12}C and ^{13}C acetaldehyde (I. Smirnov et al. 2014; L. Margulès et al. 2015), as well as thioacetaldehyde (L. Margulès et al. 2020), where the principle axis method presents serious challenges with fitting spectra since its convergence strongly depends on the ρ-value (I. Kleiner 2010). In these cases, a correct interpretation of the ground state rotational spectrum within a large range of J and K_a quantum numbers requires a global analysis including excited torsional states.

In the present study, we used the theoretical model based on the rho-axis method (RAM; B. Kirtman 1962; R. Lees & J. Baker 1968; E. Herbst et al. 1984). The main advantage of the RAM Hamiltonian is its general approach that simultaneously takes into account the A- and E-symmetry species and all the torsional levels, intrinsically taking the intertorsional interactions into account within the rotation–torsion manifold of energy levels. This method is particularly suitable for a difficult case of low barrier to internal rotation (V. V. Ilyushin et al. 2004) and/or when large coupling between internal and overall rotation occurs (I. Smirnov et al. 2014). Because this method has been presented in great detail in the literature (J. T. Hougen et al. 1994; I. Kleiner 2010) and used previously for a number of molecules with internal rotors (V. V. Ilyushin et al. 2010, 2013; I. Smirnov et al. 2014), we do not describe it here. We employed the RAM36 (RAM for three- and sixfold barriers) code that uses the RAM approach for the molecules with the C_{3v} top attached to a molecular frame of C_s or C_{2v} symmetry and having three- or sixfold barriers to internal rotation, respectively. A general expression for the RAM Hamiltonian implemented in this code as well as further details of the used theoretical approach may be found in V. V. Ilyushin et al. (2010, 2013). The RAM36 code was modified to take

into account the quadrupole hyperfine structure of the transitions that is present due to the nonzero electric quadrupole moment of the nitrogen atom. More details about this code called RAM36hf can be found in A. Belloche et al. (2017). The code is publicly available.[7]

First, we refitted the assigned rotational transitions of nitrosomethane from previous studies (D. Coffey et al. 1968; P. H. Turner & A. P. Cox 1978) using the RAM36hf program, which allowed us to reproduce the data with their original experimental accuracy. Notably, earlier studies provided only a limited model of the rotational spectrum of nitrosomethane, relying either on the internal axes method (D. Coffey et al. 1968) or the principal axes method (P. H. Turner & A. P. Cox 1978). While these models and also calculation capacities of that time yielded a relatively accurate description of the $K_a = 0$, 1 levels of the A tunneling substate, they showed significant deviations, ranging from hundreds of kHz to tens of MHz, for higher K_a values and the E substate. The absence of an adequate fitting code using the RAM approach is the primary reason why previous studies were insufficient to provide accurate spectral predictions of nitrosomethane and for an unambiguous search for this molecule in the ISM.

Using predictions obtained from the initial RAM36hf fit, we assigned and fitted the ^aR transitions in a usual bootstrap manner, with numerous cycles of refinement of the parameter set while the new data were gradually added. Then, ^bR and ^bQ lines were searched for and could be assigned carefully considering the dense spectra and their much smaller intensities. As mentioned in the experimental part, the first measurements were done using chirped-pulse spectroscopy. Lot of broad lines could be observed, due to unresolved hyperfine splitting. This is why we decided to remeasure part of the spectra with the absorption spectroscopy with better resolution. Following assignment of the ground state, we went through assignment of the first torsional state—its band origin is lying at 131 cm^{-1} (A. J. Barnes et al. 1976; E. K. Dolgov et al. 2004), giving relative intensities to the ground state at room temperature of 0.53. The analysis of the first torsional state stabilized the fit and reduced the correlation between torsional parameters of the RAM Hamiltonian models.

The complete data set treated at the final stage of the current study includes both our new data and data from the literature. Ultimately, we assigned 778 transitions for the $v_t = 0$ state and 587 transitions for $v_t = 1$ with the maximum values $J = 30$ and $K_a = 15$. Taking line blending into account, the assigned transitions together represent a data set of 1196 distinct frequency lines. The final data set contains both the data from previous studies (D. Coffey et al. 1968; P. H. Turner & A. P. Cox 1978) and new assignments in the millimeter- and submillimeter-wave ranges. A total of 1279 lines for $v_t = 0$ and 1 states of A and E symmetries were fitted with an rms deviation of 41.1 kHz (wrms = 0.76). The final fit is based on the RAM Hamiltonian model that includes 42 parameters. The values of the molecular parameters obtained from the final fits are presented in Table 1, where they are compared with the parameters from the fit of the previous studies' data (D. Coffey et al. 1968; P. H. Turner & A. P. Cox 1978) using the RAM Hamiltonian and RAM36hf code. The primary terms of the torsional–rotational Hamiltonian, associated with the kinetic energy of the rigid rotor (A, B, C, D_{ab}), the torsional motion (ρ), and the potential energy (V_3), exhibit good agreement between both fits. However, higher-order parameters show some variations, which is expected given the number of fitted parameters and transitions.

The initial fit required 15 parameters to reproduce 83 lines within experimental accuracy, yielding a ratio of $83/15 \approx 5.5$ lines per adjustable parameter. This ratio is suboptimal for nonlinear least-squares fitting and can lead to strong correlations among parameters. Consequently, certain fitted parameters may be considered effective rather than strictly physical. In contrast, the final fit incorporates 1279 distinct frequency lines, improving this ratio fivefold. This enhancement provides a more statistically robust determination of parameters and reduces correlation effects. In particular, the inclusion of the rotational transitions in the $v_t = 1$ state allowed us to remove the strong correlation between F and ρ parameters of the Hamiltonian and to accurately determine the V_6 parameter. Part of the new measurements with the fit residuals are given in Table 2. Owing to its large size, the complete version of the global fit (Table 2) is supplied online only.

In Figure 1, we also provide the assignment of nitrosomethane rotational transitions based on the RAM Hamiltonian model. Notably, in addition to the standard a-type transitions for E-symmetry states, we observe "forbidden" x-type transitions for A symmetry states. This effect is indicative of strong rotation–torsion coupling, resulting in significant wave function mixing that influences the labeling of rotational levels in terms of K_a quantum number (V. Ilyushin 2004). This highlights the necessity of an appropriate modeling approach, such as the one employed in this study. All assigned transitions shown in Figure 1 were fitted within their experimental accuracy.

Spectral predictions for astronomical use were calculated using the set of RAM Hamiltonian parameters presented in the last column of Table 1. The predictions include the rotational transitions of the ground and first excited torsional states of CH_3NO calculated at 300 K for J values up to 95 and in the frequency range up to 400 GHz. In addition, we provide in Table 3 the tabulated values for the torsional–rotational partition function $Q_{tr}(T)$, calculated from first principles, i.e., via direct summation over the torsional–rotational states. The calculated partition function accounts for all rotational levels with $J \leqslant 100$ and all torsional levels with $v_t \leqslant 8$. The vibrational partition function was not considered as only one vibrationally excited state lies below 1000 cm^{-1}, the CNO bending mode at 574 cm^{-1} (A. J. Barnes et al. 1976; E. K. Dolgov et al. 2004). The results of the fit are available in the supplementary material associated with this article. The predicted spectra are available in different formats including standard .cat format (H. M. Pickett 1972) from the new database of the Lille spectroscopy group called the Lille Spectroscopic Database (LSD).[8] The predictions can be generated using various options (e.g., intensity units, temperature, and frequency range) that provide additional flexibility in the data access.

It should be noted that the $Q_{tr}(T)$ values presented in Table 1 do not include the spin degeneracy factor $g_I = 3$ associated with the nitrogen nuclear quadrupole hyperfine structure. In the LSD, the predicted rotational spectrum of nitrosomethane

[7] http://info.ifpan.edu.pl/~kisiel/introt/introt.htm#ram36

[8] https://lsd.univ-lille.fr

Table 1
Molecular Parameters of CH_3NO Obtained with the RAM36HF Program

ntr[a]	Parameter[b]	Operator[c]	Value[d,e]	Value from this Study[d]
220	F	p_α^2	7.540555(fixed)	7.63387(79)
220	V_3	$\frac{1}{2}(1-\cos 3\alpha)$	394.441(19)	416.39(12)
211	ρ	$J_a p_\alpha$	0.353013(61)	0.35200474(79)
202	$A_{\rm RAM}$	J_a^2	2.017751(13)	2.0240868(23)
202	$B_{\rm RAM}$	J_b^2	0.396939(16)	0.3965943(20)
202	$C_{\rm RAM}$	J_c^2	0.341918(13)	0.34160507(57)
202	D_{ab}	$\{J_a, J_b\}$	−0.1542815(30)	−0.155241(17)
440	V_6	$\frac{1}{2}(1-\cos 6\alpha)$	⋯	−24.92(22)
440	F_m	p_α^4	⋯	$-0.297(30)) \times 10^{-3}$
431	ρ_m	$J_a p_\alpha^3$	⋯	$0.789(42) \times 10^{-3}$
422	F_J	$J^2 p_\alpha^2$	⋯	$-0.705(22) \times 10^{-5}$
422	F_K	$J_a^2 p_\alpha^2$	⋯	$-0.1093(22) \times 10^{-2}$
422	F_{bc}	$p_\alpha^2(J_b^2 - J_c^2)$	⋯	$0.851(48) \times 10^{-5}$
422	V_{3J}	$J^2(1-\cos 3\alpha)$	$-0.1012(65) \times 10^{-1}$	$0.3202(29) \times 10^{-3}$
422	V_{3K}	$J_z^2(1-\cos 3\alpha)$	⋯	$-0.20475(13) \times 10^{-1}$
422	V_{3ab}	$\frac{1}{2}(1-\cos 3\alpha)\{J_a, J_b\}$	⋯	$0.5095(42) \times 10^{-2}$
422	V_{3bc}	$(J_b^2 - J_c^2)(1-\cos 3\alpha)$	⋯	$0.1541(11) \times 10^{-3}$
422	D_{3ac}	$\frac{1}{2}\sin 3\alpha\{J_a, J_c\}$	⋯	$0.1569(18) \times 10^{-1}$
422	D_{3bc}	$\frac{1}{2}\sin 3\alpha\{J_b, J_c\}$	⋯	$-0.602(26) \times 10^{-3}$
413	ρ_J	$J^2 J_a p_\alpha$	$0.218(27) \times 10^{-4}$	$-0.929(18) \times 10^{-5}$
413	ρ_K	$J_a^3 p_\alpha$	⋯	$0.6847(54) \times 10^{-3}$
413	ρ_{ab}	$\frac{1}{2}p_\alpha\{J_a^2, J_b\}$	⋯	$-0.1152(98) \times 10^{-4}$
413	ρ_{bc}	$\frac{1}{2}p_\alpha\{J_a, (J_b^2 - J_c^2)\}$	⋯	$-0.264(49) \times 10^{-5}$
404	Δ_J	$-J^4$	$0.359(22) \times 10^{-6}$	$0.38510(74) \times 10^{-6}$
404	Δ_{JK}	$-J^2 J_a^2$	$-0.72(10) \times 10^{-5}$	$-0.5315(71) \times 10^{-5}$
404	Δ_K	$-J_a^4$	$0.252(16) \times 10^{-4}$	$0.16219(49) \times 10^{-3}$
404	δ_J	$-2J^2(J_b^2 - J_c^2)$	$0.05231(20) \times 10^{-6}$	$0.7275(10) \times 10^{-7}$
404	δ_K	$-\{J_a^2, (J_b^2 - J_c^2)\}$	$0.344(14) \times 10^{-6}$	$0.1162(43) \times 10^{-5}$
404	D_{abK}	$\{J_a, J_b\}J_a^2$	⋯	$0.1500(59) \times 10^{-4}$
660	V_9	$\frac{1}{2}(1-\cos 9\alpha)$	⋯	3.09(20)
642	V_{6J}	$J^2(1-\cos 6\alpha)$	⋯	$0.953(25) \times 10^{-4}$
642	V_{6ab}	$\frac{1}{2}\{J_a, J_b\}(1-\cos 6\alpha)$	⋯	$0.483(33) \times 10^{-3}$
642	D_{6ac}	$\frac{1}{2}(\cos 6\alpha)\{J_a, J_c\}$	⋯	$-0.1146(36) \times 10^{-2}$
624	D_{3acK}	$\frac{1}{2}\{J_a, J_c\}J_a^2$	⋯	$-0.670(58) \times 10^{-6}$
624	V_{3abJ}	$\frac{1}{2}(1-\cos 3\alpha)\{J_a, J_b\}J^2$	⋯	$0.13337(84) \times 10^{-6}$
624	V_{3JJ}	$J^4(1-\cos 3\alpha)$	⋯	$-0.1077(80) \times 10^{-7}$
624	V_{3b4c4}	$\frac{1}{2}(1-\cos 3\alpha)(J_b^4 + J_c^4)$	⋯	$-0.501(85) \times 10^{-8}$
606	Φ_J	J^6	⋯	$0.1623(61) \times 10^{-12}$
606	$\Phi_{\rm KJ}$	$J^2 J_z^4$	⋯	$-0.1960(68) \times 10^{-9}$
606	ϕ_J	$2J^4(J_b^2 - J_c^2)$	⋯	$0.263(16) \times 10^{-12}$
⋯	χ_{aa}	⋯	$0.49(11) \times 10^{-4}$	$0.43(15) \times 10^{-4}$
⋯	χ_{bb}	⋯	$-0.2207(53) \times 10^{-3}$	$-0.2181(71) \times 10^{-3}$
	Number of fitted parameters		15	43
	Number of transitions $v_t = 0$, $v_t = 1$		114, 0	885, 587
	Distinct frequency lines		83	1279
	$F_{\rm max}$ in GHz		40	660
	$J_{\rm max}$, $K_{a,\rm max}$		29, 4	30, 15
	rms in kHz		97.4	41.1
	wrms unitless		0.65	0.76

Notes.
[a] $n = t + r$, where n is the total order of the operator, t is the order of the torsional part, and r is the order of the rotational part.
[b] Parameter nomenclature based on the subscript procedures of L.-H. Xu et al. (2008).
[c] $\{A, B, C\} = ABC + CBA$, $\{A, B\} = AB + BA$. The product of the operator in the third column of a given row and the parameter in the second column of that row gives the term actually used in the torsional–rotational Hamiltonian of the program, except for F, ρ, and $A_{\rm RAM}$, which occur in the Hamiltonian in the form $F(p_\alpha - \rho P_a)^2 + A_{\rm RAM} P_a^2$.
[d] All values are in cm^{-1} (except ρ, which is unitless). Statistical uncertainties are shown as one standard uncertainty in the units of the last two digits.
[e] The parameters obtained with a refit of the data from D. Coffey et al. (1968) and P. H. Turner & A. P. Cox (1978).

is available in two separate entries: one that accounts for nuclear hyperfine structure and one that does not. The partition function in Table 1 is suitable for use with the latter. For the former, the values in Table 1 should be multiplied by $g_I = 3$.

4. Astronomical Observations: Search for CH_3NO

With the newly measured and analyzed spectra, we have searched for this molecule toward the cold dark cloud TMC-1 as well as the high-mass star-forming regions Sgr B2(N) and NGC 6334I. Details of each individual search are provided in the following subsections. The molecular signal of CH_3NO was not observed in any of the sources, and 3σ column density upper limits were determined. For this analysis, the spectra were simulated with the `molsim` Python package (B. A. McGuire et al. 2024) under the assumption that the molecular signal is described by a single excitation temperature. The observational parameters (i.e., source size, excitation temperature, and linewidth) are listed in Table 4; these values were mainly adapted from B. A. McGuire et al. (2019). The lines used to derive the upper limits are shown in Figure 3. The determined column density upper limits are then displayed in Table 5.

4.1. TMC-1

TMC-1 is a cold molecular cloud with an extensive, well-characterized molecular inventory, generally dominated by relatively large unsaturated carbon-chain molecules (i.e., B. A. McGuire et al. 2017a; A. M. Burkhardt et al. 2018; R. A. Loomis et al. 2021). A wide variety of cyclic and aromatic molecules have also been observed in this source (B. A. McGuire et al. 2018b, 2021; J. Cernicharo et al. 2021, 2024b; M. L. Sita et al. 2022; D. Loru et al. 2023; G. Wenzel et al. 2024, 2025). These detected species generally have cold excitation temperatures ranging from 5 to 10 K and narrow linewidths ($\sim$0.3 km s^{-1}). The observational data analyzed in this work are from the fourth data reduction of the GBT Observations of TMC-1: Hunting Aromatic Molecules (GOTHAM) project on the Robert C. Byrd Green Bank Telescope (GBT; M. L. Sita et al. 2022). These observations center on TMC-1's cyanopolyyne peak at (J2000) $\alpha = 04^{\rm h}41^{\rm m}42\overset{\rm s}{.}50$ $\delta = +25°41'26\overset{''}{.}8$. The frequency coverage is from 7.9 to 36.4 GHz. There are a few frequency gaps, however, owing to a lack of receiver coverage. The rms noise level of the observations generally ranges from approximately 2 to 20 mK, and the frequency resolution is 1.4 kHz. With these high-spectral-resolution observational data and narrow spectral lines, we would expect to be able to resolve some of the hyperfine structure of CH_3NO. However, as mentioned previously, molecular emission is not observed toward this source. Assuming an excitation temperature of 7 K, a $v_{\rm lsr}$ of 5.8 km s^{-1} and a linewidth of 0.3 km s^{-1}, the 3σ upper limit column density of CH_3NO was determined to be 3.68×10^{12} cm^{-2}. Figure 4 displays the matched filter response resulting from the velocity stack of the CH_3NO spectrum toward TMC-1. This approach has been applied to identify several other molecules in the GOTHAM data, even when their molecular signals are weak in the observations (R. A. Loomis et al. 2021). However, no matched filter response is observed for CH_3NO, indicating that there is no evidence that molecular signal for this species is present in the data. The lower-energy isomer NH_2CHO has been detected in numerous sources but not in a cold cloud such as TMC-1. Past searches for this species have resulted in an upper limit of $\sim 5 \times 10^{11}$ cm^{-2} (A. López-Sepulcre et al. 2015), almost 1 order of magnitude lower than the upper limit for CH_3NO derived in this work. The species HNCO and HCNO, possible precursors to NH_2CHO and CH_3NO, have been detected in a number of cold clouds including TMC-1; however, the derived column densities of HCNO are primarily on the order of 1×10^{10} cm^{-2} and 1–2 orders of magnitude lower than the corresponding HNCO column densities (N. Marcelino et al. 2008; J. Cernicharo et al. 2024a). Thus, a large abundance of CH_3NO, greater than that of NH_2CHO, is unlikely, and the derived CH_3NO upper limit does not provide a critical constraint.

4.2. NGC 6334I

NGC 6334I is a prominent star-forming region within the molecular cloud complex NGC 6334. This source is known to contain several individual protostellar sources (T. R. Hunter et al. 2006; C. L. Brogan et al. 2016; T. R. Hunter et al. 2017). The observational spectra investigated here were collected using the Atacama Large Millimeter/submillimeter Array (ALMA) and extracted from a position toward the MM1 hot core (J2000 $\alpha = 17^{\rm h}20^{\rm m}53\overset{\rm s}{.}387$ $\delta = -35°46'57\overset{''}{.}533$). These observations are very dense, and previous research has demonstrated that this region hosts a diverse array of complex chemicals, including several large oxygen-containing molecules (B. A. McGuire et al. 2017b, 2018a; Z. T. P. Fried et al. 2024). The observations cover a range of frequencies across ALMA Bands 4, 7, 9, and 10. The parameters for the Band 9 and 10 observations are presented in B. A. McGuire et al. (2018a). The Band 7 and Band 4 observational parameters are then detailed by B. A. McGuire et al. (2017b) and Z. T. P. Fried et al. (2024), respectively. The data were smoothed using the standard CASA `imsmooth` routine to ensure that the observations in each frequency band had an angular resolution of $0\overset{''}{.}26 \times 0\overset{''}{.}26$. The molecular emission toward this source was simulated with an excitation temperature of 225 K, a $v_{\rm lsr}$ of -5.2 km s^{-1}, and a linewidth of 3 km s^{-1} (N. F. W. Ligterink et al. 2020). Since the observations are line confusion limited, we derived the upper limit column density using the reported rms of the observations. Given that the line used for this determination falls within ALMA Band 9, the rms noise level was measured at 50 mJy beam^{-1} (T. R. Hunter et al. 2021). Ultimately, a 3σ column density upper limit of 1.17×10^{16} cm^{-2} was determined. The column density of the ^{13}C isotopologue of the lower-energy isomer NH_2CHO toward this pointing position in NGC 6334I was found to be 3.2×10^{16} cm^{-2} (N. F. W. Ligterink et al. 2020). Assuming the ^{12}C/^{13}C ratio of 62 that was determined for NGC 6334I (E. G. Bøgelund et al. 2018), this would suggest a NH_2CHO column density around 2×10^{18} cm^{-2}. Thus, the upper limit of CH_3NO indicates that this species is at least a few hundred times less abundant than its more stable isomer.

4.3. Sgr B2(N)

Sagittarius B2(N), also known as Sgr B2(N), is a region within the Sagittarius B2 molecular cloud where high-mass star

Table 2
Measured Frequencies of the CH_3NO Residuals from the Fit[a]

Upper Level						Lower Level						Frequency (Unc.) (in MHz)	o.-c. (in MHz)
Sy″[b]	m″[c]	F″[d]	J″	K_a''	K_c''	Sy′	m′	F′	J′	K_a'	K_c'		
A_2	0	−1.0	30	5	25	A_1	0	−1.0	29	5	24	654398.1870(0.0500)	−0.0017
E	1	−1.0	30	5	25	E	1	−1.0	29	5	24	654480.0610(0.0500)	0.0026
A_1	−3	−1.0	30	4	27	A_2	−3	−1.0	29	4	26	654921.8710(0.0500)	0.0204
A_2	−3	−1.0	30	5	26	A_1	−3	−1.0	29	5	25	655531.9540(0.0500)	0.0579
A_1	−3	−1.0	30	5	25	A_2	−3	−1.0	29	5	24	656324.4290(0.0500)	−0.0496
A_2	−3	−1.0	30	2	28	A_1	−3	−1.0	29	2	27	657767.3800(0.0500)	0.0824
E	1	−1.0	30	2	28	E	1	−1.0	29	2	27	657997.2520(0.0500)	0.0131
A_1	0	−1.0	30	2	28	A_2	0	−1.0	29	2	27	658062.2190(0.0500)	−0.0252
E	−2	−1.0	30	2	28	E	−2	−1.0	29	2	27	659111.3890(0.0500)	0.0769
E	−2	−1.0	30	4	26	E	−2	−1.0	29	4	25	659632.6550(0.0500)	−0.0132

Notes.
[a] Table 2 is published in its entirety in the electronic edition of the Astrophysical Journal. Only its portion is shown here for guidance regarding its form and content.
[b] Symmetry in the G6 group.
[c] Free rotor quantum number.
[d] For unblended hyperfine structure, F is fixed to −1.0.

(This table is available in its entirety in machine-readable form in the online article.)

Table 3
Torsional–Rotational Partition Functions at Various Temperatures

T (K)	$Q(T)_{rot\_tors}$
300	44240.9104
220	22539.3584
170	13085.0097
150	10131.8393
70	2480.5037
40	1017.6146
20	358.3883
10	127.3921

Table 4
Assumed Observational Parameters for CH_3NO toward TMC-1, Sgr B2(N), and NGC 6334I

Source	Telescope	θ_s[a] (″)	ΔV (km s^{-1})	T_{ex} (K)
TMC-1	GBT	⋯	0.3	7
Sgr B2(N) (Hot)	GBT	2.2	7.0	150
Sgr B2(N) (Cold)	GBT	20	12.0	5
NGC 6334I	ALMA	⋯	3.0	225

Note.
[a] If a source size is not listed, it is assumed that the source fills the beam.

formation is actively occurring. This region contains several hot core sources, which have demonstrated remarkable chemical complexity through various line surveys (A. Belloche et al. 2013, 2016, 2019). In part due to high column densities of these hot core sources, it has become a rich hunting ground for detecting less abundant complex species (A. Belloche et al. 2019). In fact, a number of notable complex organic molecules were first discovered in this interstellar source (J. M. Hollis et al. 2000; A. Belloche et al. 2008). Other molecules have been observed in absorption within the cold molecular shell surrounding the hot cores (B. A. McGuire et al. 2016). Our observational data toward this source are from the Prebiotic Interstellar Molecular Survey (PRIMOS) project on the GBT, for which the observational details are provided by J. L. Neill et al. (2012). In short, this survey was collected toward the pointing position (J2000) $\alpha = 17^h47^m19\overset{s}{.}8$ $\delta = -28°22'17''$ and has an almost continuous frequency coverage from 1 to 50 GHz. Both warm emission lines and cold absorption lines can be seen in the data; we therefore searched for CH_3NO in both of these temperature regimes. The assumed source parameters for both the hot and cold components are listed in Table 4. We ultimately derived a column density upper limit of 2.18×10^{17} cm^{-2} for a hot component in the core of Sgr B2(N) and 1.36×10^{13} cm^{-2} in the cold molecular shell. This upper limit is similar to the determined column densities of other fairly small nitrogen containing species in absorption in the PRIMOS data, as E-cyanomethanimine (HNCHCN) was detected at a column density of 1.5×10^{13} cm^{-2} (D. P. Zaleski et al. 2013). E- and Z-ethanimine (CH_3CHNH) were also observed with column densities on the order of 10^{13} cm^{-2} (R. A. Loomis et al. 2013).

5. Interstellar Chemistry of CH_3NO

As mentioned previously, CH_3NO is a higher-energy isomer of formamide, a precursor to prebiotic molecules that has been detected in numerous star-forming regions including Sgr B2(N) and NGC 6334I (A. López-Sepulcre et al. 2019). In the gas phase, formamide can be formed from the barrierless reaction between NH_2 radicals and formaldehyde (H_2CO; V. Barone et al. 2015). The analogous reaction between CH_3 radicals and HNO, which has been detected in the ISM, is endothermic to form CH_3NO, whereas the competing H-abstraction channel is strongly exothermic and occurs along the minimum energy path (Y. M. Choi & M. C. Lin 2005). Nitrous acid (HONO) is another known interstellar molecule containing an NO bond and is known to react with CH_3; however, the CH_3NO product channel is endothermic and requires crossing sizable activation barriers (M. E. Fuller & C. F. Goldsmith 2019). The gas-phase reactions of CH_3 with the nitrogen oxides NO and NO_2 have been investigated experimentally and theoretically in the context of combustion

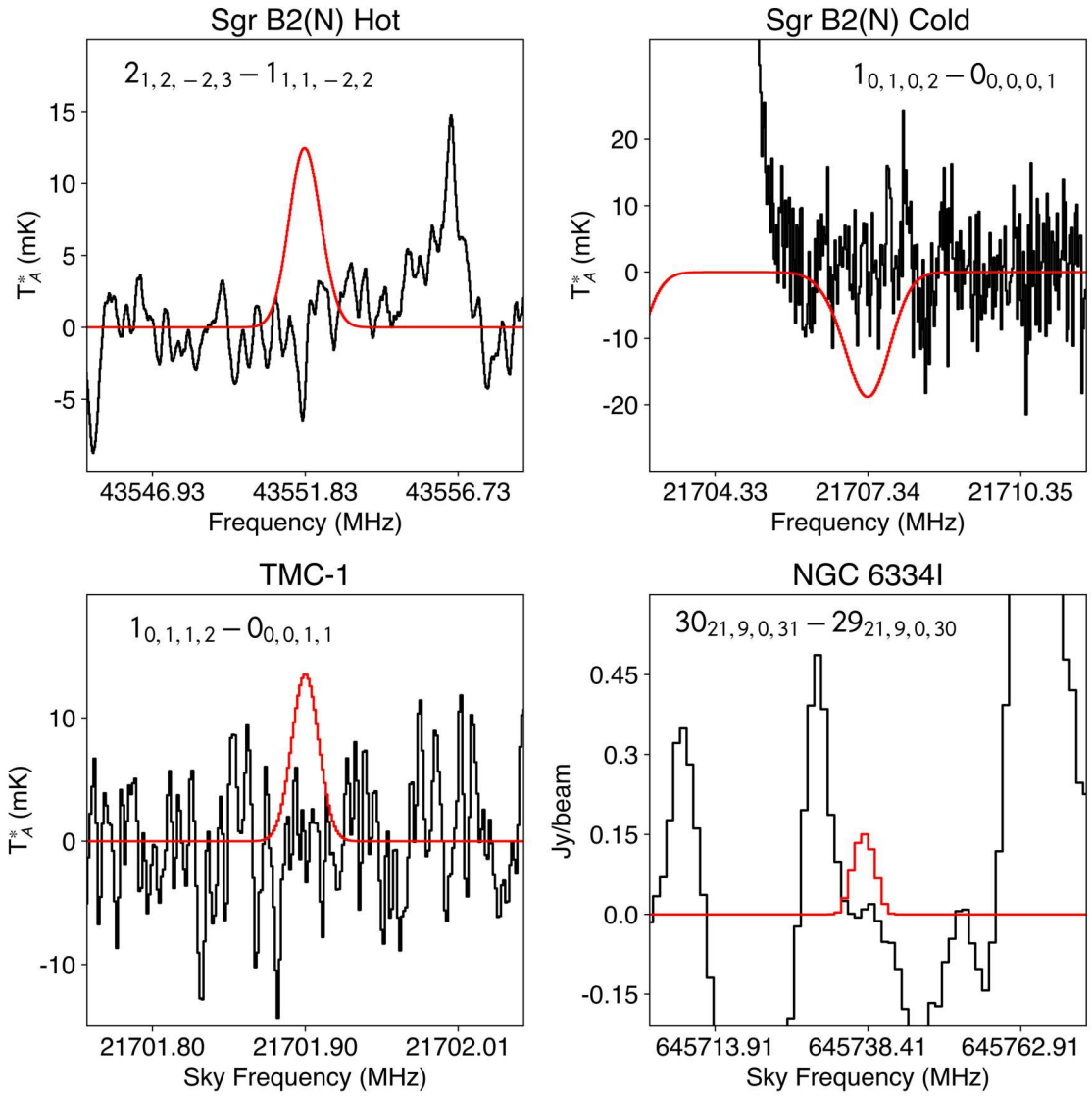

Figure 3. Transitions used to determine the upper limit column densities of CH_3NO. The simulated spectrum of CH_3NO is depicted in red and overlaid on top of the observational data (black). The observational data toward Sgr B2(N) are already velocity corrected, so no velocity shift was applied to the simulation. For the observations toward Sgr B2(N) and NGC 6334I, several transitions are encapsulated under the simulated line; therefore, the listed quantum numbers are for the encapsulated transitions with the greatest line strength. The quantum numbers are labeled as follows: $J_{K_a,K_c,m,F}$.

and atmospheric chemistry. The potential energy surface of the reaction of CH_3 with NO_2 shows a number of possible bimolecular product channels accessible through submerged barriers, but CH_3NO is not one of them (J.-X. Zhang et al. 2005). Conversely, the reaction between CH_3 and NO involves several large barriers leading to bimolecular products but a barrierless formation of the initial CH_3NO complex (T. Wolff & H. G. Wagner 1988; J.-X. Zhang et al. 2005); thus, a radiative association mechanism may be feasible under the low-temperature and density conditions of the ISM.

The UV photodissociation of nitromethane (CH_3NO_2) has been studied in the collisionless gas phase and in nitromethane ices along with energetic electron processing. CH_3NO is not a major product of the gas-phase decomposition (L. J. Butler et al. 1983); however, energetic processing of nitromethane ices has resulted in the formation of CH_3NO as well as CH_3NO dimers and carbene insertion products (R. I. Kaiser & P. Maksyutenko 2015; P. Maksyutenko et al. 2015). It is not known whether nitromethane can efficiently form on interstellar grains. Consecutive H-atom additions to fulminic acid (HCNO), a known interstellar molecule, have been proposed and investigated by B. Keresztes et al. (2023) as a grain-surface route to formaldoxime (H_2CNOH), an isomer of CH_3NO. Using a 3.1 K para-H_2 matrix in conjunction with quantum chemical calculations, the authors found that H_2CNO can be efficiently formed from H-addition to HCNO, but further hydrogenation is unable to compete with H-abstraction via hydrogen atoms back to HCNO. Energetic processing of H-, C-, N-, and O-containing ices often results in the formation of formamide with no evidence of CH_3NO (A. López-Sepulcre et al. 2019), possibly due to the greater stability of the former species compared to the latter as well as the lack of precursors containing N–O bonds. Methanol-NO ices irradiated with energetic electrons have found to predominantly yield methyl nitrite (CH_3ONO), likely from the recombination of CH_3O and NO (S. Góbi et al. 2018). CH_3NO may thus be formed in ices

Table 5
Column Density Upper Limits of CH_3NO and the Transition Parameters Used

Source	Frequency[a] (MHz)	Upper Level[b] J'', K_a'', K_c'', m'', F''	Lower Level[b] J', K_a', K_c', m', F'	E_u (K)	$S_{ij}\mu^2$ (Debye^2)	T_b[c] (mK)	N_T (cm^{-2})
TMC-1	21701.90	1 0 1 1 2	0 0 0 1 1	1.14	2.83	4.5	$\leqslant 3.68 \times 10^{12}$
Sgr B2(N) (Hot)	43551.83	2 1 2 -2 3	1 1 1 -2 2	206.47	3.57	4.2	$\leqslant 2.18 \times 10^{17}$
Sgr B2(N) (Cold)	21707.34	1 0 1 0 2	0 0 0 0 1	1.04	2.83	6.3	$\leqslant 1.36 \times 10^{13}$
NGC 6334I	645738.41	30 21 9 0 31	29 21 9 0 30	95.94	29.69	50[d]	$\leqslant 1.17 \times 10^{16}$

Notes.
[a] Velocity-shifted frequency of the line in the observational data. The PRIMOS data toward Sgr B2(N) that were used for the analysis were already velocity corrected; therefore, no v_{lsr} shift was applied to the simulation.
[b] For the observations toward Sgr B2(N) and NGC 6334I, the linewidth covers several transitions The line parameters listed here are for the encapsulated component with the greatest line strength.
[c] For the TMC-1 and Sgr B2(N) observations, this is the 1σ rms noise around the line used to determine the upper limit. Since the NGC 6334I observations are line confusion limited, the reported rms noise of the ALMA Band 9 observations was used (T. R. Hunter et al. 2021).
[d] Units of mJy/beam.

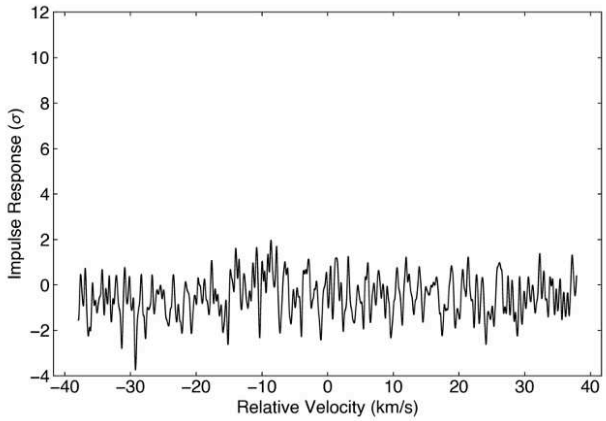

Figure 4. Matched filter impulse response determined by cross-correlating the velocity-stacked line profile of CH_3NO (using the simulation parameters detailed in the text) and the velocity-stacked observational spectrum from the GOTHAM data toward TMC-1.

containing both NO and CH_3 radicals through the aforementioned reaction between these species.

As mentioned previously, now that the spectrum of this molecule has been measured and analyzed across a broadband frequency range extending into the submillimeter-wave regime, it can be reliably searched for in various other interstellar sources. Notable candidates include the G +0.693 − 0.027 molecular cloud, where hydroxylamine, a compound containing an N–O bond, has been detected (V. M. Rivilla et al. 2020). Another promising source is the IRAS 16293-2422B hot corino, where numerous methyl-containing nitrogenated or oxygenated species, along with HONO—which also features an N–O bond—have been observed (J. K. Jørgensen et al. 2018; A. Coutens et al. 2019).

6. Conclusion

Reinvestigation of the rotational spectrum of CH_3NO was carried out in the frequency range of 150–660 GHz in order to provide accurate predictions for astronomical searches. The rotational transitions of the ground and first excited torsional states were assigned up to $J = 30$ and fit using an RAM Hamiltonian within experimental accuracy. The overall weighted rms deviation of the global fit of 2035 line frequencies is 0.76, indicating that we have an appropriate set of parameters to provide reliable predictions for astronomical observations. Unfortunately, our first attempt to search for CH_3NO toward the cold dark cloud TMC-1 as well as the high-mass star-forming regions Sgr B2(N) and NGC 6334I was not successful. We provide 3σ column density upper limits in the different sources. Based on our results, frequency predictions for astrophysical use were produced up to 660 GHz and are available on the LSD.

Acknowledgments

This work was supported by the Programme National "Physique et Chimie du Milieu Interstellaire" (PCMI) of CNRS/INSU with INC/INP cofunded by CEA and CNES. The authors acknowledge support from the MIT International Science and Technology Initiatives (MISTI) and the MISTI Seed Fund, MIT-France Program. B.A.M. was supported in part by National Science Foundation grant AST-2205126. The National Radio Astronomy Observatory is a facility of the National Science Foundation operated under cooperative agreement by Associated Universities, Inc. Z.T.F.P. and B.A.M. acknowledge support from Schmidt Family Futures. A.N.B. acknowledges support from the National Science Foundation grant No. 2141064. This paper makes use of the following ALMA data: ADS/JAO.ALMA#2017.1.00661.S, ADS/JAO.ALMA#2013.1.00278.S, and ADS/JAO.ALMA#2012.1.00712.S. ALMA is a partnership of ESO (representing its member states), NSF (USA), and NINS (Japan), together with NRC (Canada), MOST and ASIAA (Taiwan), and KASI (Republic of Korea), in cooperation with the Republic of Chile. The Joint ALMA Observatory is operated by ESO, AUI/NRAO, and NAOJ. J.-C.G. thanks the Centre National d'Etudes Spatiales (CNES) for a grant.

ORCID iDs

Laurent Margulès https://orcid.org/0000-0003-0629-8277
Zachary T. P. Fried https://orcid.org/0000-0001-5020-5774
Alex N. Byrne https://orcid.org/0000-0002-4593-518X
Brett A. McGuire https://orcid.org/0000-0003-1254-4817
Roman A. Motiyenko https://orcid.org/0000-0002-3849-1533
J.-C. Guillemin https://orcid.org/0000-0002-2929-057X

References

Barnes, A. J., Hallam, H. E., Waring, S., & Armstrong, J. R. 1976, FaTr, 72, 1
Barone, V., Latouche, C., Skouteris, D., et al. 2015, MNRAS: Letters, 453, L31
Belloche, A., Garrod, R. T., Müller, H. S. P., et al. 2019, A&A, 628, A10
Belloche, A., Menten, K. M., Comito, C., et al. 2008, A&A, 482, 179
Belloche, A., Meshcheryakov, A. A., Garrod, R. T., et al. 2017, A&A, 601, A49
Belloche, A., Müller, H. S. P., Garrod, R. T., & Menten, K. M. 2016, A&A, 587, A91
Belloche, A., Müller, H. S. P., Menten, K. M., Schilke, P., & Comito, C. 2013, A&A, 559, A47
Bhujle, V., Wild, U., Baumann, H., & Wagniere, G. 1976, Tetrahedron, 32, 467
Brogan, C. L., Hunter, T. R., Cyganowski, C. J., et al. 2016, ApJ, 832, 187
Burkhardt, A. M., Herbst, E., Kalenskii, S. V., et al. 2018, MNRAS, 474, 5068
Butler, L. J., Krajnovich, D., Lee, Y. T., Ondrey, G. S., & Bersohn, R. 1983, JChPh, 79, 1708
Bøgelund, E. G., McGuire, B. A., Ligterink, N. F. W., et al. 2018, A&A, 615, A88
Cernicharo, J., Agúndez, M., Cabezas, C., et al. 2024a, A&A, 682, L4
Cernicharo, J., Agúndez, M., Cabezas, C., et al. 2021, A&A, 649, L15
Cernicharo, J., Cabezas, C., Fuentetaja, R., et al. 2024b, A&A, 690, L13
Choi, Y. M., & Lin, M. C. 2005, International Journal of Chemical Kinetics, 37, 261
Christie, M. I. 1959a, RSPSA, 249, 248
Christie, M. I. 1959b, RSPSA, 249, 258
Coffey, D., Jr, Britt, C. O., & Boggs, J. E. 1968, JChPh, 49, 591
Coutens, A., Ligterink, N. F. W., Loison, J.-C., et al. 2019, A&A, 623, L13
DePrince, A. E., & Mazziotti, D. A. 2010, JChPh, 133, 034112
Dolgov, E. K., Bataev, V. A., & Godunov, I. A. 2004, IJQC, 96, 193
Fried, Z. T. P., El-Abd, S. J., Hays, B. M., et al. 2024, ApJL, 965, L23
Frost, D., Lau, W., McDowell, C., & Westwood, N. 1982, JPhCh, 86, 3577
Fuller, M. E., & Goldsmith, C. F. 2019, PComI, 37, 695
Gowenlock, B., & Lüttke, W. 1958, Quarterly Reviews, Chemical Society, 12, 321
Góbi, S., Crandall, P. B., Maksyutenko, P., Förstel, M., & Kaiser, R. I. 2018, JPCA, 122, 2329
Herbst, E., Messer, J., De Lucia, F. C., & Helminger, P. 1984, JMoSp, 108, 42
Hollis, J. M., Lovas, F. J., & Jewell, P. R. 2000, ApJ, 540, L107
Hougen, J. T., Kleiner, I., & Godefroid, M. 1994, JMoSp, 163, 559
Hunter, T. R., Brogan, C. L., De Buizer, J. M., et al. 2021, ApJL, 912, L17
Hunter, T. R., Brogan, C. L., MacLeod, G., et al. 2017, ApJL, 837, L29
Hunter, T. R., Brogan, C. L., Megeath, S. T., et al. 2006, ApJ, 649, 888
Ilyushin, V. 2004, JMoSp, 227, 140
Ilyushin, V. V., Alekseev, E., Dyubko, S., Kleiner, I., & Hougen, J. T. 2004, JMoSp, 227, 115
Ilyushin, V. V., Endres, C. P., Lewen, F., Schlemmer, S., & Drouin, B. J. 2013, JMoSp, 290, 31
Ilyushin, V. V., Kisiel, Z., Pszczókowski, L., Mäder, H., & Hougen, J. T. 2010, JMoSp, 259, 26
Jørgensen, J. K., Müller, H. S. P., Calcutt, H., et al. 2018, A&A, 620, A170
Kaiser, R. I., & Maksyutenko, P. 2015, CPL, 631, 59
Keresztes, B., Góbi, S., Csonka, I. P., et al. 2023, MNRAS, 521, 2649
Kirtman, B. 1962, JChPh, 37, 2516
Kleiner, I. 2010, JMoSp, 260, 1
Kolesniková, L., Alonso, E., Mata, S., & Alonso, J. 2017, JMoSp, 335, 54
Kolesniková, L., Tercero, B., Alonso, E., et al. 2018, A&A, 609, A24
Lattelais, M., Pauzat, F., Ellinger, Y., & Ceccarelli, C. 2010, A&A, 519, A30
Lees, R., & Baker, J. 1968, JChPh, 48, 5299
Ligterink, N. F. W., El-Abd, S. J., Brogan, C. L., et al. 2020, ApJ, 901, 37
Liszt, H., & Turner, B. 1978, ApJL, 224, L73
Long, J. A., Harris, N. J., & Lammertsma, K. 2001, JOrgC, 66, 6762
Loomis, R. A., Burkhardt, A. M., Shingledecker, C. N., et al. 2021, NatAs, 5, 188
Loomis, R. A., Zaleski, D. P., Steber, A. L., et al. 2013, ApJL, 765, L9
Loru, D., Cabezas, C., Cernicharo, J., Schnell, M., & Steber, A. L. 2023, A&A, 677, A166
López-Sepulcre, A., Balucani, N., Ceccarelli, C., et al. 2019, ESC, 3, 2122
López-Sepulcre, A., Jaber, A. A., Mendoza, E., et al. 2015, MNRAS, 449, 2438
Maksyutenko, P., Muzangwa, L. G., Jones, B. M., & Kaiser, R. I. 2015, PCCP, 17, 7514
Marcelino, N., Cernicharo, J., Tercero, B., & Roueff, E. 2008, ApJL, 690, L27
Margulès, L., Ilyushin, V., McGuire, B., et al. 2020, JMoSp, 371, 111304
Margulès, L., Motiyenko, R. A., Ilyushin, V. V., & Guillemin, J. C. 2015, A&A, 579, A46
McGuire, B. A. 2022, ApJS, 259, 30
McGuire, B. A., Brogan, C. L., Hunter, T. R., et al. 2018a, ApJL, 863, L35
McGuire, B. A., Burkhardt, A. M., Kalenskii, S., et al. 2018b, Sci, 359, 202
McGuire, B. A., Burkhardt, A. M., Shingledecker, C. N., et al. 2017a, ApJL, 843, L28
McGuire, B. A., Carroll, P. B., Loomis, R. A., et al. 2016, Sci, 352, 1449
McGuire, B. A., Loomis, R. A., Burkhardt, A. M., et al. 2021, Sci, 371, 1265
McGuire, B. A., Shingledecker, C. N., Willis, E. R., et al. 2017b, ApJL, 851, L46
McGuire, B. A., Shingledecker, C. N., Willis, E. R., et al. 2019, ApJ, 883, 201
McGuire, B. A., Xue, C., Lee, K. L. K., El-Abd, S., & Loomis, R. A. 2024, molsim, v0.5.0, Zenodo, doi:10.5281/zenodo.12697227
Miller, D., & Steacie, E. 1951, JChPh, 19, 73
Motiyenko, R. A., Armieieva, I. A., Margulès, L., Alekseev, E. A., & Guillemin, J.-C. 2019, A&A, 623, A162
Neill, J. L., Muckle, M. T., Zaleski, D. P., et al. 2012, ApJ, 755, 153
Pickett, H. M. 1972, JChPh, 56, 1715
Rivilla, V. M., Martín-Pintado, J., Jiménez-Serra, I., et al. 2020, ApJL, 899, L28
Rubin, R., Swenson, G., Jr, Benson, R., Tigelaar, H., & Flygare, W. 1971, ApJL, 169, L39
Sita, M. L., Changala, P. B., Xue, C., et al. 2022, ApJL, 938, L12
Smirnov, I., Alekseev, E., Ilyushin, V., et al. 2014, JMoSp, 295, 44
Turner, P. H., & Cox, A. P. 1978, FaTr, 74, 533
Ulich, B., Hollis, J., & Snyder, L. 1977, ApJL, 217, L105
Wenzel, G., Cooke, I. R., Changala, P. B., et al. 2024, Sci, 386, 810
Wenzel, G., Speak, T. H., Changala, P. B., et al. 2025, NatAs, 9, 262
Wolff, T., & Wagner, H. G. 1988, Berichte der Bunsengesellschaft für physikalische Chemie, 92, 678
Xu, L.-H., Fisher, J., Lees, R., et al. 2008, JMoSp, 251, 305
Zakharenko, O., Motiyenko, R. A., Margulès, L., & Huet, T. R. 2015, JMoSp, 317, 41
Zaleski, D. P., Seifert, N. A., Steber, A. L., et al. 2013, ApJL, 765, L10
Zhang, J.-X., Liu, J.-Y., Li, Z.-S., & Sun, C.-C. 2005, JCoCh, 26, 807
Ziurys, L., Apponi, A., Hollis, J., & Snyder, L. 1994, ApJL, 436, L181
Zou, L., Guillemin, J.-C., Motiyenko, R. A., & Margulès, L. 2021, A&A, 649, A60
Zou, L., Motiyenko, R. A., Margulès, L., & Alekseev, E. A. 2020, RSciI, 91, 063104